

## Seebeck coefficients of $\text{Fe}_{3-y}\text{Ti}_y\text{O}_4$ and $\text{Fe}_{3-x}\text{Zn}_x\text{O}_4$ single crystals and their interpretation

D. Kim\* and J. M. Honig

*Department of Chemistry, Purdue University, West Lafayette, Indiana 47907-1393*

(Received 14 June 1993; revised manuscript received 30 September 1993)

Seebeck coefficient data have been measured for  $\text{Fe}_{3-y}\text{Ti}_y\text{O}_4$  and for  $\text{Fe}_{3-x}\text{Zn}_x\text{O}_4$  single crystals in the range 75–300 K and for  $0 \leq y \leq 0.9$  and  $0 \leq x \leq 0.29$ . The data have been rationalized in terms of a small polaron model, on the basis of an adaptation of the standard order-disorder theory. Very good agreement is obtained between the two-parameter theory and experiment. In this model the Ti sites do not participate in electronic conduction.

### INTRODUCTION

As part of an ongoing study concerning the electrical properties of doped magnetites we report here on the thermoelectric properties of the  $\text{Fe}_{3-y}\text{Ti}_y\text{O}_4$  system. We also reevaluate and provide a theoretical analysis of present and earlier data on the  $\text{Fe}_{3-x}\text{Zn}_x\text{O}_4$  system. Taken in conjunction with recent conductivity measurements<sup>1</sup> a reasonably consistent picture of electrical transport in  $\text{Fe}_{3(1-\delta)}\text{O}_4$ ,  $\text{Fe}_{3-x}\text{Zn}_x\text{O}_4$ , and  $\text{Fe}_{3-y}\text{Ti}_y\text{O}_4$  is beginning to emerge.

### EXPERIMENTAL

The  $\text{Fe}_{3-y}\text{Ti}_y\text{O}_4$  and  $\text{Fe}_{3-x}\text{Zn}_x\text{O}_4$  single-crystal specimens were synthesized and prepared for electrical measurements as described in earlier reports.<sup>2,3</sup> Special care was taken to ensure a 4/3 oxygen/cation stoichiometry.<sup>4</sup> Thermoelectric studies were carried out using an automated temperature relaxation technique<sup>5,6</sup> employed for similar measurements on  $\text{Fe}_{3(1-\delta)}\text{O}_4$ . The maximum temperature difference between the ends of the sample was 3 K; four traces of the linear voltage change with temperature were averaged to obtain a single value of the Seebeck coefficient at each temperature of the measurements.

### PRESENTATION OF DATA

We show in Figs. 1(a) and 1(b) the variation of Seebeck coefficient  $\alpha$  with temperature  $T$  for  $\text{Fe}_{3-y}\text{Ti}_y\text{O}_4$  in the composition ranges  $0 \leq x \leq 0.007$  and  $0.007 \leq x \leq 0.166$ , respectively. As has been repeatedly demonstrated,<sup>5-7</sup>  $\text{Fe}_{3(1-\delta)}\text{O}_4$ ,  $\text{Fe}_{3-y}\text{Ti}_y\text{O}_4$ , and  $\text{Fe}_{3-x}\text{Zn}_x\text{O}_4$ , undergo a first-order Verwey transition in the range  $T_v = 121$ –106 K with increasing cation vacancy density, titanium content, or zinc doping in the range below  $3\delta = x = y = 0.012$ ; the various resistivity curves, including the discontinuities at  $T = T_v$  were found to superpose well with the correspondence  $3\delta = x = y$ . Beyond a critical value  $\delta = \delta_c = 0.0039$  the above compounds were observed to undergo a second- or higher-order Verwey transition at temperatures in the range 101–82 K, which diminished with increasing  $\delta$ ,  $x$ , or  $y$  up to  $\delta = 3\delta_c$ . Beyond this point the Verwey transition disappeared altogether.

This trend is also reflected in the present Seebeck data. In Fig. 1(a) the Seebeck coefficients of  $\text{Fe}_{3-y}\text{Ti}_y\text{O}_4$  exhibit discontinuities at the temperature  $T = T_v$  of the Verwey transition;  $T_v$  diminishes linearly with increasing  $y$ . For  $T > T_v$ ,  $\alpha$  remains in the range  $-50$  to  $-58 \mu\text{V}/\text{K}$ , almost independent of temperature. For  $T < T_v$ ,  $\alpha$  drops linearly with diminishing temperature, except for the undoped specimen which exhibits an upturn below 75 K.

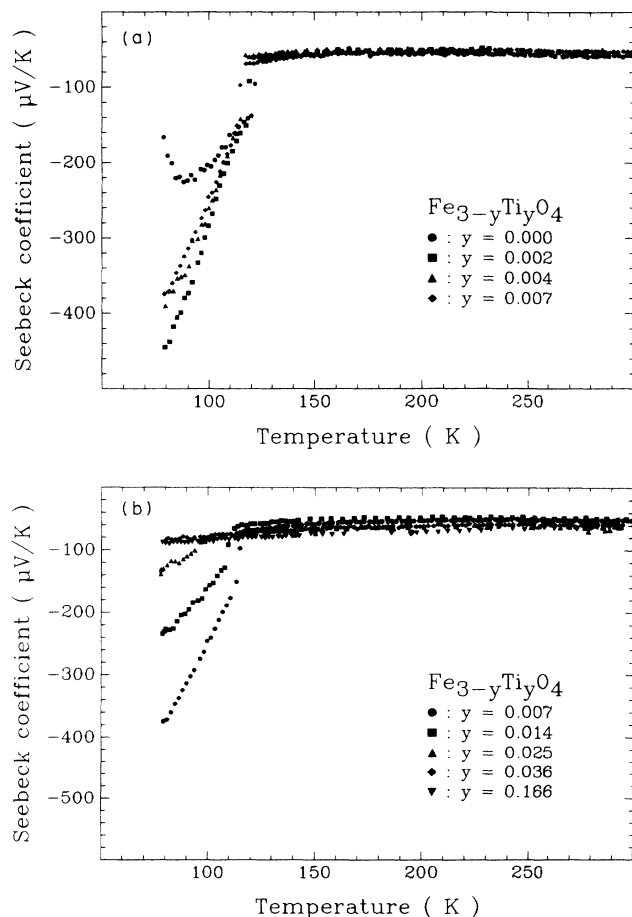


FIG. 1. Measured Seebeck coefficients versus temperature for  $\text{Fe}_{3-y}\text{Ti}_y\text{O}_4$ . (a) For very dilute titanomagnetites,  $0 \leq y \leq 0.007$ . (b) For titanomagnetites at low doping levels,  $0.007 \leq y \leq 0.166$ .

The present data set is in very good agreement with the earlier work by Kuipers and Brabers,<sup>8</sup> who explained the upturn in terms of a two-level model as arising from residual impurities. These results are consistent with a first-order transition. In Fig. 1(b) there is a discontinuity in the slope of the Seebeck coefficients at  $T_v$ . The general features of the  $\alpha(T)$  variation above and below  $T_v$  of Fig. 1(a) are also present in Fig. 1(b), including the trend of a diminishing slope in the straight line portions below  $T_v$  as the titanium content rises.

We show in Fig. 2 the variation of  $\alpha$  with  $T$  for samples with a higher Ti content in the range  $0.35 \leq y \leq 0.90$ . One should note the observed trend:  $\alpha$  becomes progressively more positive as  $y$  is increased, and the slope  $\alpha'(T)$  of the curves changes from positive below  $y \approx 0.5$  to negative above this value. In the lowest temperature range, where a rapid upturn occurs, the Seebeck measurements of titanomagnetites with  $y \geq 0.5$  are suspect; for the sample impedance then becomes comparable to that of the measuring equipment. These data are comparable to those published in a very recent investigation by Brabers<sup>9</sup> whose measurements extend up to nearly 1200 K. These are rationalized in terms of a range of localized states. We have not been able to locate other prior investigations of the Seebeck coefficient in titanomagnetites for the range of temperatures below 300 K. A publication by Trestman-Matts *et al.*<sup>9</sup> deals with such measurements above 600°C.

As a further test of the theory presented below we also include in Fig. 3 the variation of  $\alpha$  with  $T$  for a series of zinc ferrite samples  $\text{Fe}_{3-x}\text{Zn}_x\text{O}_4$  in the range  $0 < x < 0.30$ ; the present data are in excellent agreement with those published earlier.<sup>5</sup> Work by Srinivasan and Srivastava<sup>10</sup> and by Samokhvalov and Rustamov<sup>11</sup> are also in good agreement with the above results, as are the measured room-temperature Seebeck coefficients by earlier investigators.<sup>12</sup>

Preliminary to the theoretical analysis it is necessary to ascertain the cation distribution which prevails in the titanomagnetite and zinc ferrite series without cation va-

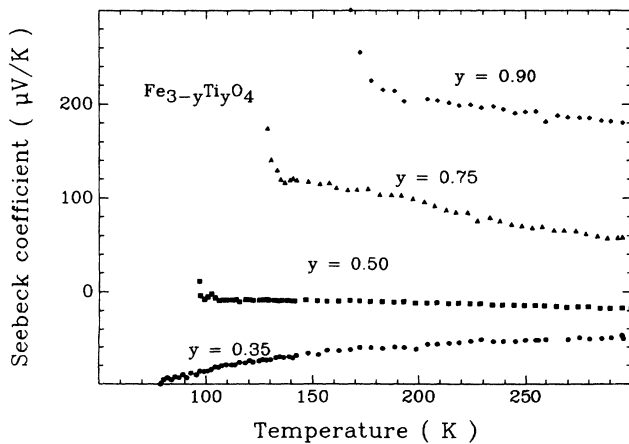


FIG. 2. Measured Seebeck coefficients versus temperature for  $\text{Fe}_{3-y}\text{Ti}_y\text{O}_4$  for titanomagnetites in the composition range  $0.35 \leq y \leq 0.90$ .

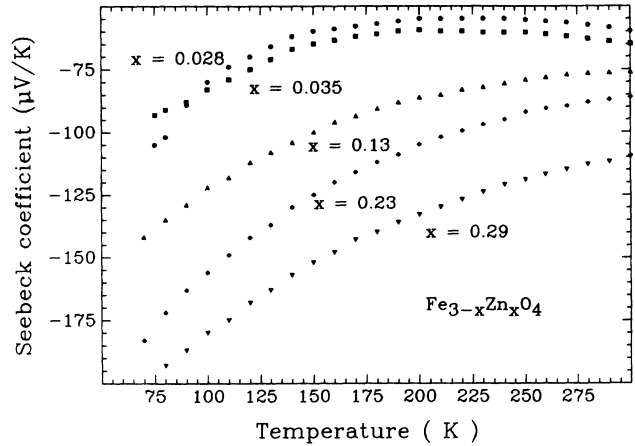


FIG. 3. Measured Seebeck coefficients versus temperature for  $\text{Fe}_{3-x}\text{Zn}_x\text{O}_4$  in the composition range  $0.028 \leq x \leq 0.29$ .

cancies. From magnetization measurements, mass, and charge balance data one arrives at the following distributions<sup>13</sup>:

$$\text{I: } (\text{Fe}^{3+})[\text{Fe}_{1-2y}^{3+}\text{Fe}_{1+y}^{2+}\text{Ti}_y^{4+}]\text{O}_4 \quad (0 \leq y \leq 0.2),$$

$$\text{II: } (\text{Fe}_{1.25-1.25y}^{3+}\text{Fe}_{1.25y-0.25}^{2+}) \\ [\text{Fe}_{0.75-0.75y}^{3+}\text{Fe}_{1.25-0.25y}^{2+}\text{Ti}_y^{4+}]\text{O}_4 \quad (0.2 < y \leq 1),$$

$$\text{III: } (\text{Fe}_{1-x}^{3+}\text{Zn}_x^{2+})[\text{Fe}_{1+x}^{3+}\text{Fe}_{1-x}^{2+}]\text{O}_4 \quad (0 \leq x \leq 1).$$

The cations enclosed by round and square brackets represents species located in tetrahedrally and octahedrally coordinated cationic interstices. The above results differ to some extent from those provided by earlier investigators.<sup>14</sup> There are some problems associated with all of the distributions because of possible spin canting and spin-glass behavior. Thus, the above distribution, which is used for consistency, is likely only on approximation to the real distribution.

One should note that  $\text{Ti}^{4+}$  displaces iron solely in octahedral interstices (*o* sites) whereas  $\text{Zn}^{2+}$  displaces  $\text{Fe}^{3+}$  solely in tetrahedrally coordinated sites (*t* sites). In principle, electronic conduction could occur through valence fluctuations of ions located on *o* sites in I, II, and III; also, via charge fluctuations of ions on *t* sites in II and III, and by the transfer of electrons from *t* to *o* sites or vice versa in I, II, and III. However, valence fluctuations on *t* sites are highly unlikely in III because of the stability of the zinc cation in its divalent state. In II charge transport by carriers on *t* sites is much less likely than that on *o* sites because of the greater cation separation distance of the *t* sites. The *o-t* interchange in II is energetically unfavorable: the spin direction of the sixth electron on  $\text{Fe}^{2+}$  in the *o* environment is opposite that of the five 3*d* core electrons of  $\text{Fe}^{3+}$  resident on *o* sites. The spin of the sixth electron is, however, parallel to that of the five 3*d* electrons of  $\text{Fe}^{3+}$  on the *t* sites. An *o-t* electron transfer without spin flip would therefore violate Hund's rule, in contrast to the *o-o* type electron transfer. An electron transfer with spin flip requires additional energy. Accordingly, we assume that only electron fluctuations among octahedral sites need be taken into account.

## MODEL FOR INTERPRETATION OF DATA

We base the subsequent model for the interpretation of the above data on an adaptation of order-disorder theory<sup>15</sup> which was used earlier in the study of the Verwey transition in magnetite.<sup>16</sup> This very elementary approach is based on the assumption that charge transport involves an activated hopping process of carriers among nearest neighbors of the octahedrally coordinated cationic interstices. In dealing with electron transfers among *o* sites one must take into account the availability of empty sites [ $\text{Fe}^{3+}$ ] adjacent to an occupied one [ $\text{Fe}^{2+}$ ]. The probability of achieving such a configuration in turn depends on the interactions between electrons placed on adjacent sites, and on the Ti or Zn content of the samples. The latter in turn governs the charge-carrier density.

The most primitive way of taking these various factors into account is by subdividing the lattice sites up into three categories as shown in the top part of Table I, namely,  $\otimes$  (type C),  $\circ$  (type A), and  $\bullet$  (type B). As indicated in the table, for the titanomagnetites series the C, A, and B units represent octahedrally coordinated interstices occupied by  $\text{Ti}^{4+}$ ,  $\text{Fe}^{3+}$ , and  $\text{Fe}^{2+}$  ions, respectively. For zinc ferrites C, A, and B represent octahedrally coordinated interstices occupied respectively by  $\text{Fe}^{2+}$  in which a trapped charge-carrier resides in a deformed lattice position, by  $\text{Fe}^{3+}$ , and by  $\text{Fe}^{2+}$  containing a mobile charge carrier. Charge-carrier interactions among nearest neighbors are then taken into account by considering pairs of nearest-neighbor octahedral sites such as C-C, C-B, C-A, and the like. These possible site pairings are listed in the bottom part of Table I. The theoretical treatment now brings the machinery of order-disorder theory to bear on the problem. In this approach one forms a total of  $ZL/2$  octahedral site pairs (also called "bonds") from  $L$  lattice points (octahedrally coordinated interstices), where  $Z=6$  is the number of nearest-neighbor sites. This representative collection already contains  $ZL$  individual sites (also called "points"); the overcount is corrected for by introducing a second collection of  $(1-Z)L$  individual sites, such that the combined collection of sites and points tallies properly.

The various possible occupation states of the points and bonds are exhibited in Table I for use with both the titanomagnetite and zinc ferrite series. Several items should be noted: (i) The tabulation contains a complete listing of possible bond configurations; however, only the sets associated with the three lowest-energy states are selected for further consideration. It is possible to construct a theory involving all six configurations, but this would entail the use of five adjustable energy parameters.<sup>17</sup> The aim in the present treatment is to ascertain whether a two-parameter theory, involving only the selected configurations shown in the table suffices for the analysis of the Seebeck coefficient data. (ii) Only two possible resonance states, namely, BA and AB are shown on line 8 and 9 of Table I, whereas no interchange of CB and BC (line 5) or of CA and AC (line 6) are indicated. This is based on the fact that the charge carrier (designated by the closed circle, state B) can interchange position with an empty site (open circle, state A); this is the precursor to the directed drift of charge carriers in an applied electric field. No such interchange is possible for the other two configurations. (iii) For titanomagnetites configuration C (the crossed circle) represents a titanium atom located on an octahedral site. For zinc ferrites, configuration C represents a charge carrier localized by self-trapping in the ground-state configuration. This particular CA state was invoked, along with states AB, BA, and BB, in modeling the features of the Verwey transition in undoped  $\text{Fe}_{3(1-\delta)}\text{O}_4$ .<sup>16</sup>

Before proceeding we note that the various probabilities shown in Table I are not all independent. One must take into account the normalization requirements

$$\beta_2 + 2\beta_1 + \beta_0 = 1, \quad (1)$$

$$\gamma_2 + \gamma_1 + \gamma_0 = 1, \quad (2)$$

as well as the consistency relation for mobile electrons (filled circles),

$$\beta_2 + \beta_1 = \gamma_2 \quad (3)$$

and a requirement based on the composition of the material under study, namely

TABLE I. Tabulation of possible configurations for representative assemblies, together with probability and energy parameters.

Symbol	Designation	Titanomagnetites			Zinc ferrites		
			Probability	Energy		Probability	Energy
$\otimes$	C	$\text{Ti}^{4+}$	$\gamma_0$	$\epsilon_C$	$\text{Fe}^{2+ \text{ a}}$	$\gamma_0$	$\epsilon_C$
$\circ$	A	$\text{Fe}^{3+}$	$\gamma_1$	$\epsilon_A$	$\text{Fe}^{3+}$	$\gamma_1$	$\epsilon_A$
$\bullet$	B	$\text{Fe}^{2+}$	$\gamma_2$	$\epsilon_B$	$\text{Fe}^{2+}$	$\gamma_2$	$\epsilon_B$
$\otimes - \otimes$	CC						
$\otimes - \bullet$	CB						
$\otimes - \circ$	CA		$\beta_0$	$\epsilon_{CA}$		$\beta_0$	$\epsilon_{Ca}$
$\bullet - \bullet$	BB		$\beta_2$	$\epsilon_{BB}$		$\beta_2$	$\epsilon_{BB}$
$\bullet - \circ$	BA		$\beta_1$	$\epsilon_{BA}$		$\beta_1$	$\epsilon_{BA}$
$\circ - \bullet$	AB		$\beta_1$	$\epsilon_{AB}$		$\beta_1$	$\epsilon_{AB}$
$\circ - \circ$	AA						

<sup>a</sup>Charge carrier trapped by lattice deformations.

$$\gamma_0 = c \text{ or } \gamma_1 = c, \quad (4)$$

where  $c$  is the density of  $\text{Ti}^{4+}$  ions or of  $\text{Fe}^{3+}$  ions. From the six probabilities of Table I we now arbitrarily select  $\beta_2$  and  $\gamma_2$  as the set of independent variables.

### THEORETICAL DEVELOPMENT

To interpret the experimental Seebeck coefficient measurements in  $\text{Ti}_y\text{Fe}_{3-y}\text{O}_4$  and  $\text{Zn}_x\text{Fe}_{3-x}\text{O}_4$  we adopt the following procedure: First we set up expressions for the energy  $E_b$  of the bond figure assemblies and for the energy  $E_s$  of the site figure assemblies, by consulting the entries for the probability and energy parameters shown in Table I. We now obtain, in view of Eqs. (1) and (2),

$$\begin{aligned} E_b &= \frac{Z}{2}L(\beta_2\epsilon_{\text{BB}} + 2\beta_1\epsilon_{\text{AB}} + \beta_0\epsilon_{\text{CA}}) \\ &= \frac{Z}{2}L(\beta_2U + 2\beta_1E + \epsilon_{\text{CA}}), \end{aligned} \quad (5a)$$

where

$$U \equiv \epsilon_{\text{BB}} - \epsilon_{\text{CA}} \equiv U(\beta_2) \text{ and } E \equiv \epsilon_{\text{AB}} - \epsilon_{\text{CA}} \equiv E(\beta_1). \quad (5b)$$

For the point figure assembly we find

$$\begin{aligned} E_s &= (1-Z)L(\gamma_2\epsilon_{\text{B}} + \gamma_1\epsilon_{\text{A}} + \gamma_0\epsilon_{\text{C}}) \\ &= (1-Z)L(\gamma_2\epsilon_2 + \gamma_1\epsilon_1 + \epsilon_{\text{C}}), \end{aligned} \quad (6)$$

where  $\epsilon_2 \equiv \epsilon_{\text{B}} - \epsilon_{\text{C}}$  and  $\epsilon_1 \equiv \epsilon_{\text{A}} - \epsilon_{\text{C}}$ .

The corresponding entropies in Stirling's approximation are given by

$$S_b = -k_B \frac{Z}{2}L(\beta_2 \ln \beta_2 + 2\beta_1 \ln \beta_1 + \beta_0 \ln \beta_0) \quad (7)$$

for the bond figure assembly, and by

$$S_s = -k_B(1-Z)L(\gamma_2 \ln \gamma_2 + \gamma_1 \ln \gamma_1 + \gamma_0 \ln \gamma_0) \quad (8)$$

for the site figure assembly. One may now construct the free energy from the expression

$$F = F_b + F_s = E_b + E_s - T(S_b + S_s). \quad (9)$$

Next we introduce the equilibrium constraint by minimizing  $F$  through the requirement

$$\frac{\partial F}{\partial \beta_2} \equiv \frac{\partial F_b}{\partial \beta_2} = 0.$$

Here one must keep in mind that  $\beta_1 = \gamma_2 - \beta_2$  and  $\beta_0 = 1 - 2\gamma_2 + \beta_2$  are themselves functions of  $\beta_2$ . We find

$$\begin{aligned} 0 &= \frac{Z}{2}L \left[ \beta_2 U' + U + 2E \frac{\partial \beta_1}{\partial \beta_2} + 2\beta_1 E' \frac{\partial \beta_1}{\partial \beta_2} \right] \\ &\quad + k_B T \frac{Z}{2}L \left[ \ln \beta_2 + 2(\ln \beta_1) \frac{\partial \beta_1}{\partial \beta_2} + (\ln \beta_0) \frac{\partial \beta_0}{\partial \beta_2} + 1 \right. \\ &\quad \left. + 2 \frac{\partial \beta_1}{\partial \beta_2} + \frac{\partial \beta_0}{\partial \beta_1} \right], \end{aligned} \quad (10)$$

which may be rewritten as

$$\begin{aligned} \ln(\beta_2 \beta_0 / \beta_1^2) &= -[(U - 2E) + \beta_2 U' - 2\beta_1 E'] / k_B T \\ &\equiv -R / k_B T \end{aligned} \quad (11a)$$

or as

$$\beta_2 \beta_0 / \beta_1^2 = e^{-R/k_B T} \equiv C. \quad (11b)$$

We next substitute for  $\beta_0$  and  $\beta_1$  in Eq. (11b) and solve the resulting quadratic expression for

$$\beta_2 = [2(1-C)]^{-1}[-S + \sqrt{S^2 + 4C(1-C)\gamma_2^2}], \quad (12a)$$

with

$$S \equiv 1 - 2\gamma_2(1-C), \quad (12b)$$

so that  $\beta_2$  is now specified in terms of  $\gamma_2$ . For purposes of obtaining Seebeck coefficients we next determine the chemical potential of movable charge carriers according to the relation  $\mu = \partial \tilde{F} / \partial \gamma_2$ , with  $\tilde{F} \equiv F/L$ ,

$$\begin{aligned} \mu &= \frac{\partial \tilde{F}}{\partial \gamma_2} = \frac{\partial \tilde{F}_b}{\partial \gamma_2} + \frac{\partial \tilde{F}_s}{\partial \gamma_2} = (1-Z)\epsilon_2 + Z(\gamma_2 - \beta_2)E' + ZE + k_B T(1-Z) \ln[\gamma_2 / (1 - \gamma_1 - \gamma_2)] \\ &\quad + k_B TZ \ln[(\gamma_2 - \beta_2) / (1 - 2\gamma_2 + \beta_2)]. \end{aligned} \quad (13)$$

For a collection of electrons whose kinetic energy is small the Seebeck coefficient is related to  $\mu$  via<sup>18</sup>

$$\alpha = \frac{\mu - E}{k_B T} = (Z-1) \frac{E - \epsilon_2}{k_B T} + Z \frac{(\gamma_2 - \beta_2)E'}{k_B T} + (1-Z) \ln[\gamma_2 / (1 - \gamma_1 - \gamma_2)] + Z \ln[(\gamma_2 - \beta_2) / (1 - 2\gamma_2 + \beta_2)]. \quad (14)$$

In the above  $E$  is the energy of the transport levels relative to the ground state [see Eq. (5b)]. In ordinary applications it is appropriate to set  $E = \epsilon_2$ , which then also requires that  $E' = 0$ . With these simplifications the first two terms in Eq. (14) drop out and the remaining expression [the last two terms in Eq. (14)] will be used as the basic relation for calculation of the Seebeck coefficients.

### DISCUSSION

It should be noted that our first attempts to interpret the Seebeck coefficient data in terms of an itinerant, strongly correlated electron model<sup>19</sup> ended in failure. The above experimental work can only be rationalized using a model in which charge carriers are essentially local-

ized. This is in accord with a recent high-precision x-ray-diffraction study that yielded information on the electron density distribution in magnetite.<sup>20</sup> Ihle and Lorenz<sup>21</sup> have suggested that the conductivity observed in  $\text{Fe}_3\text{O}_4$  is due to a superposition of a small polaron hopping and a polaron narrow band mechanism, the latter being dominant at low temperature. Other authors had previously suggested the dominance of the thermally activated charge carrier transport.<sup>8,22</sup> Still other workers<sup>23</sup> have interpreted the conductivity data in terms of itinerant charge carriers in band states. As is shown below, a satisfactory fit of the data is possible based solely on localized electron characteristics.

As concerns the titanomagnetite system, the data in Figs. 1(a) and 1(b) for very low degrees of Ti substitution are virtually identical with those obtained for nonstoichiometric magnetite  $\text{Fe}_{3(1-\delta)}\text{O}_4$ , with the correspondence  $y = 3\delta$  for  $y \leq 0.036$ .<sup>2</sup> The data analysis invoked in an earlier publication<sup>24</sup> may thus be taken over in totality. This previous analysis was based on a simplified version of the theory displayed above, which holds for the limiting cases  $C = 0$  and 1. It was shown that in these circumstances the resulting theory would simulate first- and second-order transitions, leading to excellent agreement with the experimental Seebeck measurements on  $\text{Fe}_{3(1-\delta)}\text{O}_4$ . Thus, no further elaboration of this approach is necessary to deal with the data of Figs. 1(a) and 1(b).

The results of Fig. 2 are simulated by carrying out numerical calculations based on the last two terms of Eq. (14), together with Eqs. (12). The parameter  $C$  was determined from Eq. (11) by assuming that  $R$  varies linearly with  $T$  as  $R = V - QT$ , with  $V \equiv U - 2E$  and, in the spirit of Landau, simulating  $\beta_2 U'$  by  $-QT$ . As is consistent with formula II, we set  $\gamma_2 = (1.25 - 0.25y)/2$  and  $\gamma_1 = (0.75 - 0.75y)/2$ . In the range  $y < 0.20$ , formula I was used, together with  $\gamma_2 = (1 + y)/2$  and  $\gamma_1 = (1 - 2y)/2$ .  $V$  and  $Q$  were then individually adjusted until the resulting calculated curves of  $\alpha(T)$  fell within the experimental error of the data. A typical set of calculations is shown in Fig. 4. Comparison with Fig. 2 indicates very

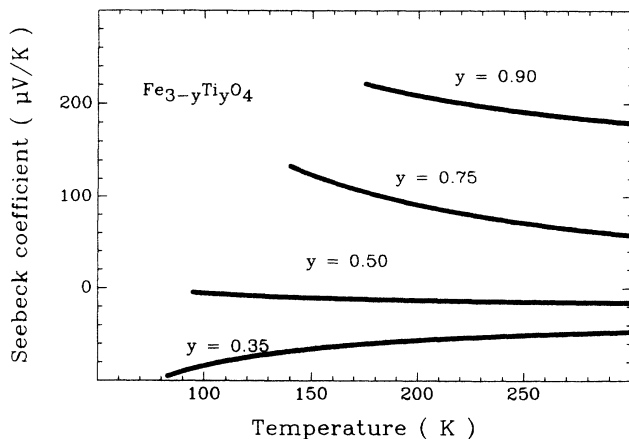


FIG. 4. Calculated variation of Seebeck coefficient with temperature for titanomagnetites; compare with Fig. 2.

good agreement between theory and experiment. Note the assumption that  $\text{Ti}^{4+}$  sites are not accessible to the conduction carriers. This is in agreement with the conclusion detailed in Ref. 1, based on conductivity trends. Furthermore, the temperature variations of  $\alpha$ , which change systematically with increasing Ti content, are correctly reproduced by our elementary theory.

A diagrammatic representation of the appropriate  $V$  and  $Q$  values in the  $Q$ - $V$  parameter space is shown in Fig. 5. The narrow ellipses show the ranges in  $V$  and  $Q$  for which the calculated and experimental curves agree within experimental error. The uncertainties increase with  $y$ . There is no clear trend in the variation of  $V$  and  $Q$  with increasing  $y$ : for  $y \leq 0.5$ ,  $V$  is close to zero ( $U \approx 2E$ ) or slightly negative ( $U < 2E$ ), whereas for  $y > 0.5$ ,  $V$  is positive ( $U > 2E$ ). The energy difference  $|U - 2E|$  remains within the range  $-20$ – $100$  K.  $Q$  is always negative: that is, with rising temperature the "gap"  $U = \epsilon_{\text{BB}} - \epsilon_{\text{CA}}$  becomes larger. For samples of lower Ti content, as well as for the case  $y = 0.5$ , where  $\alpha$  does not change significantly with  $T$ , this temperature variation dominates  $V$ .

Analogous results are encountered for the zinc ferrites. Here, the right side of Table I is relevant. In light of formula III we now set  $\gamma_2 = (1 - x)/2$  and  $\gamma_1 = c$ , and carry out the same cycle of calculations as discussed above. A typical set of theoretical results are shown in Fig. 6. Here the agreement with experiment (Fig. 3) is satisfactory, though not as good as for the titanomagnetites, in the range  $100 < T < 300$  K. For  $T < 100$  K the calculated curves tend toward higher negative  $\alpha$  values than do the experimental measurements. The reason for this discrepancy is not clear. Either the model fails at low temperatures, possibly because charge carriers begin to assume more itinerantlike characteristics in this range,<sup>23</sup> or else the experimental measurements begin to be subject to the upswing of  $\alpha$  to less negative values at lower temperature. Such a situation is generally encountered in nonstoichiometric magnetites or zinc ferrites<sup>6,24</sup> but not in titanomagnetites.

The range of  $V$  and  $Q$  values consistent with the experimental data are shown in Fig. 7. One sees that for in-

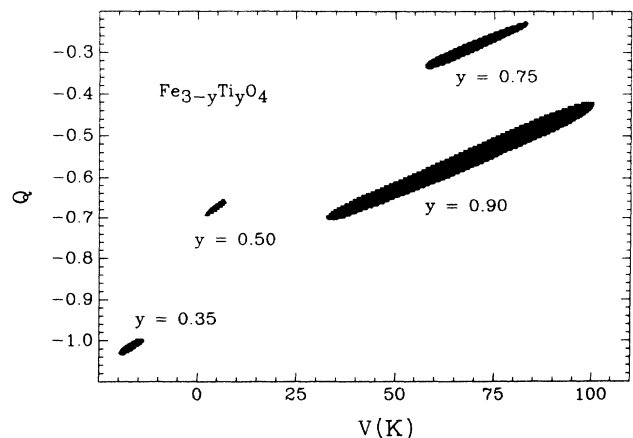


FIG. 5. Allowable variation of  $V$  and  $Q$  parameters used in calculation of Seebeck coefficients of titanomagnetites; see text.

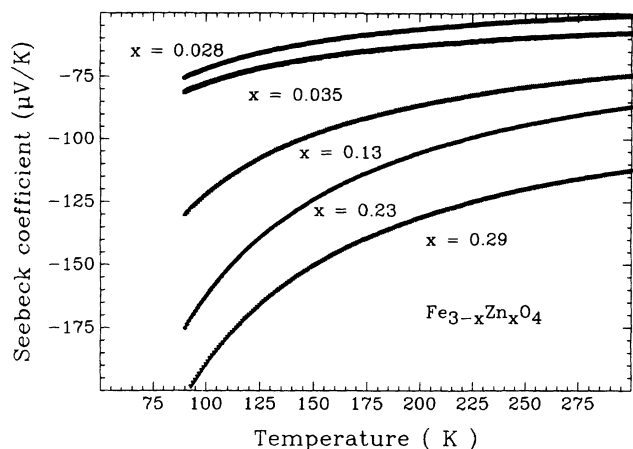


FIG. 6. Calculated variation of Seebeck coefficients of zinc ferrites; compare with Fig. 3.

creasing  $x$  in  $\text{Fe}_{3-x}\text{Zn}_x\text{O}_4$  the acceptable  $V$  values, and hence  $U-2E$ , become increasingly negative, while  $Q$ , which is now positive, changes in an irregular manner. The difference in parametrization for the titanomagnetites as compared to the zinc ferrites reflects the fact that  $\text{Ti}^{4+}$  enters the octahedrally coordinated interstices and decreases the density of sites among which the charge carriers may be distributed, whereas the presence of the  $\text{Zn}^{2+}$  in tetrahedrally coordinated interstitial positions merely adjusts the density of charge carriers on the  $o$  sites.

#### SUMMARY

Consistent with the earlier conductivity measurements<sup>1</sup> we find that the Seebeck coefficients measurements can be properly accounted for on the basis of a localized charge-carrier model. The data suggest that in

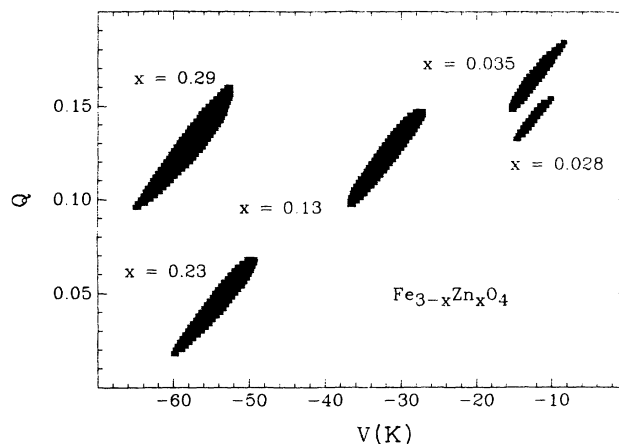


FIG. 7. Allowable variation of  $V$  and  $Q$  parameters used in calculation of Seebeck coefficients of zinc ferrites; see text.

$\text{Fe}_{3-y}\text{Ti}_y\text{O}_4$   $\text{Ti}^{4+}$  does not exhibit charge fluctuations and thus does not participate in conduction processes. The various trends in the Seebeck coefficient measurements of both  $\text{Fe}_{3-y}\text{Ti}_y\text{O}_4$  and  $\text{Fe}_{3-x}\text{Zn}_x\text{O}_4$  are correctly reproduced by a model involving charge-carrier localization, while taking account of interactions between electrons on adjacent octahedrally coordinated interstices. The theoretical analysis was carried out on the basis of a standard order-disorder model<sup>15</sup> as applied to octahedrally coordinated cation interstitialcies.

#### ACKNOWLEDGMENTS

D. K. was partially supported by a grant from the Korean Science and Engineering Foundation. This research was supported by NSF Grant No. DMR 92-22986. We thank A. Kozłowski for supplying the crystals.

\*Permanent address: Department of Natural Science, Pusan National University of Technology, 100 Yongdang, Namgu, Pusan 608-739, Korea.

<sup>1</sup>A. Kozłowski, R. Rasmussen, J. E. Sabol, P. Metcalf, and J. M. Honig, *Phys. Rev. B* **48**, 2057 (1993).

<sup>2</sup>Z. Kąkol, J. Sabol, and J. M. Honig, *J. Appl. Phys.* **69**, 4822 (1991); *Phys. Rev. B* **44**, 2198 (1991); Z. Kąkol, J. Sabol, J. Stickler, and J. M. Honig, *ibid.* **46**, 1975 (1992).

<sup>3</sup>P. Wang, M. W. Wittenauer, D. J. Buttrey, Q. W. Choi, P. Metcalf, Z. Kąkol, and J. M. Honig, *J. Cryst. Growth* **104**, 285 (1990); M. W. Wittenauer, P. Wang, P. Metcalf, Z. Kąkol, and J. M. Honig, in *Inorganic Synthesis*, edited by D. W. Murphy (Wiley, New York, in press).

<sup>4</sup>J. M. Honig and R. Aragón, *Z. Anorg. Allg. Chem.* **541**, 80 (1986); P. Wang, Q. W. Choi, and J. M. Honig, *ibid.* **550**, 91 (1987).

<sup>5</sup>P. Wang, Z. Kąkol, M. W. Wittenauer, and J. M. Honig, *Phys. Rev. B* **42**, 4553 (1990).

<sup>6</sup>R. Aragón, R. J. Rasmussen, J. P. Shepherd, J. W. Koenitzer, and J. M. Honig, *J. Magn. Mater.* **54-57**, 1335 (1986).

<sup>7</sup>J. P. Shepherd, R. Aragón, J. W. Koenitzer, and J. M. Honig,

*Phys. Rev. B* **32**, 1818 (1985); J. P. Shepherd, J. W. Koenitzer, R. Aragón, J. Spałek, and J. M. Honig, *ibid.* **43**, 8461 (1991).

<sup>8</sup>A. J. M. Kuipers and V. A. M. Brabers, *Phys. Rev. B* **20**, 594 (1979).

<sup>9</sup>V. A. M. Brabers (unpublished); A. Trestman-Matts, S. E. Dorris, S. Kumarakrishnan, and T. O. Mason, *J. Am. Ceram. Soc.* **66**, 829 (1983).

<sup>10</sup>G. Srinivasan and C. M. Srivastava, *Phys. Status Solidi B* **103**, 665 (1981).

<sup>11</sup>A. A. Samokhvalov and A. G. Rustamov, *Fiz. Tverd. Tela* **7**, 1198 (1965) [*Sov. Phys. Solid State* **7**, 961 (1965)]; M. I. Klinger and A. A. Samokhvalov, *Phys. Status Solidi B* **79**, 9 (1977).

<sup>12</sup>B. Gillot, *Phys. Status Solidi A* **69**, 719 (1987); B. Gillot and F. Jemmali, *ibid.* **77**, 339 (1988); M. A. Mousa and M. A. Ahmed, *J. Mater. Sci.* **23**, 3083 (1988).

<sup>13</sup>Z. Kąkol, J. Sabol, and J. M. Honig, *Phys. Rev. B* **43**, 649 (1991).

<sup>14</sup>S. Akimoto, T. Katsura, and M. J. Yoshida, *J. Geomagn. Geoelectr.* **9**, 165 (1957); L. Néel, *Adv. Phys.* **4**, 191 (1955); R. Chevallier, J. Bolfa, and J. Mathieu, *Bull. Soc. Fr. Minéral.*

- Cristallogr. **78**, 307 (1955); W. O'Reilly and S. K. Banerjee, Phys. Lett. **17**, 237 (1965); A. Stephenson, Geophys. J. R. Astron. Soc. **18**, 190 (1969); U. Bleil, Z. Geophys. **37**, 305 (1971); Pure Appl. Geophys. **114**, 165 (1976); V. A. M. Brabers (unpublished).
- <sup>15</sup>S. Hijmans and J. de Boer, Physica **21**, 472 (1955).
- <sup>16</sup>J. M. Honig and J. Spaček, J. Less-Common Met. **156**, 423 (1989); J. M. Honig, J. Spaček, and P. Gopalan, J. Am. Ceram. Soc. **73**, 3225 (1990); J. M. Honig and J. Spaček, J. Solid State Chem. **96**, 115 (1992).
- <sup>17</sup>H. Kloor (personal communication).
- <sup>18</sup>T. C. Harman and J. M. Honig, *Thermoelectric and Thermomagnetic Effects and Applications* (McGraw-Hill, New York, 1967), Chaps. 3 and 4; L. L. Van Zandt and J. M. Honig, J. Appl. Phys. **52**, 5625 (1981).
- <sup>19</sup>A. K. Mabatah, E. J. Yoffa, P. C. Eklund, M. S. Dresselhaus, and D. Adler, Phys. Rev. Lett. **39**, 494 (1977); Phys. Rev. B **21**, 1676 (1980); P. Kwizera, M. S. Dresselhaus, and D. Adler, *ibid.* **21**, 2328 (1980); T. Holstein, Ann. Phys. (N.Y.) **8**, 325 (1959); R. A. Bari, Phys. Rev. B **10**, 1560 (1974); G. Beni, *ibid.* **10**, 2186 (1974).
- <sup>20</sup>E. L. Belokoneva and V. G. Tsirel'son, Zh. Neorg. Khim. **37**, 154 (1992) [Russ. J. Inorg. Chem. **37**, 83 (1992)].
- <sup>21</sup>D. Ihle and B. Lorenz, J. Phys. C **18**, L647 (1985); J. Phys. C **19**, 5239 (1986).
- <sup>22</sup>W. Haubenreisser, Phys. Status Solidi B **1**, 619 (1961); D. L. Camphausen, Solid State Commun. **11**, 99 (1972); Z. Šimša, Phys. Status Solidi B **96**, 581 (1979); A. A. Samokhvalov, N. M. Tutikov, and G. P. Skorniyakov, Fiz. Tverd. Tela **10**, 2760 (1968) [Sov. Phys. Solid State **10**, 2172 (1969)]; P. Muret, Solid State Commun. **14**, 1119 (1972); U. Buchenau, Phys. Status Solidi B **70**, 181 (1975); V. A. M. Brabers, Philos. Mag. B **42**, 429 (1980); H. Kronmüller and F. Walz, *ibid.* **42**, 433 (1980); T. E. Whall, K. K. Yeung, Y. G. Proykova, and V. A. M. Brabers, *ibid.* **50**, 689 (1984).
- <sup>23</sup>J. R. Cullen and E. R. Callen, J. Appl. Phys. **41**, 879 (1970); also Phys. Rev. B **7**, 397 (1973); B. J. Evans, in *Magnetism and Magnetic Materials*, Proceedings of the 20th Annual Conference on Magnetism and Magnetic Materials, AIP Conf. Proc. No. 24, edited by C. D. Graham, Jr., G. H. Lander, and J. J. Rhyne (AIP, New York, 1975); B. J. Evans and H. N. Ok, Physica **86-88B**, 931 (1977), pp. 73ff; A. Yanase and K. Siratori, J. Phys. Soc. Jpn. **53**, 312 (1984).
- <sup>24</sup>R. Aragón and J. M. Honig, Phys. Rev. B **37**, 209 (1988); J. M. Honig, Phys. Chem. Minerals **15**, 476 (1988).